DE GRUYTER OPEN

Communications in Applied and Industrial Mathematics
ISSN 2038-0909

Research Article

Commun. Appl. Ind. Math. 7 (3), 2016, 135–161 DOI: 10.1515/caim-2016-0025

Boundary conditions for semi-Lagrangian methods for the BGK model

Maria Groppi[1*], Giovanni Russo[2*], Giuseppe Stracquadanio[1*]

[1]Dipartimento di Matematica e Informatica
Università degli Studi di Parma, Italy

[2]Dipartimento di Matematica e Informatica
Università degli Studi di Catania, Italy

[*]Email address for correspondence: giuseppe.stracquadanio@nemo.unipr.it

Communicated by Maurizio Falcone

Received on May 29, 2015. Accepted on December 16, 2015.

Abstract

A new class of high-order accuracy numerical methods based on a semi-Lagrangian formulation for the BGK model of the Boltzmann equation has been recently proposed in [1]. In this paper semi-Lagrangian schemes for the BGK equation have been extended to treat boundary conditions, in particular the diffusive ones. Two different techniques are proposed, using or avoiding iterative procedures. Numerical simulations illustrate the accuracy properties of these approaches and the agreement with the results available in literature.

Keywords: BGK equation, semi-Lagrangian methods, high-order schemes, boundary conditions

AMS subject classification: 76P05, 65M25, 65L06, 65L10.

1. Introduction.

The BGK equation, introduced by Bhatnagar, Gross and Krook [2] and independently by Welander [3] is a simplified model of the Boltzmann equation [4] and it is widely used in the kinetic theory of gases. In the BGK model the Boltzmann (integral) collision operator is replaced by a relaxation operator; the initial value problem for the distribution function $f(t,x,v)$ that at time t and at position x have velocity v reads as

$$\begin{aligned} &\frac{\partial f}{\partial t} + v\cdot\nabla_x f = Q_{BGK}[f] \equiv \frac{1}{\varepsilon}(M[f]-f), \\ &(x,v,t)\in\mathbb{R}^d\times\mathbb{R}^N\times\mathbb{R}^+, \quad f(x,v,0)=f_0(x,v), \end{aligned} \tag{1}$$

where d and N denote the dimension of the physical and velocity spaces, respectively, and ε^{-1} is the collision frequency, that, throughout this paper, is assumed to be a fixed constant for simplicity. $M[f]$ denotes the local Maxwellian with the same macroscopic moments of the distribution function $f(x,v,t)$, and is given by

$$M[f](x,v,t) = \frac{\rho(x,t)}{\left[2\pi RT(x,t)\right]^{N/2}} \exp\left(- \frac{(v-u(x,t))^2}{2RT(x,t)} \right), \tag{2}$$

where R is the ideal gas constant and $\rho(x,t) \in \mathbb{R}^+$, $u(x,t) \in \mathbb{R}^N$ and $T(x,t) \in \mathbb{R}^+$ denote the macroscopic moments of the distribution function f, that is: density, mean velocity and temperature, respectively. They are obtained in the following way

$$(\rho, \rho u, E)^T = \langle f\phi(v) \rangle, \ \phi(v) = \left(1, v, \frac{1}{2}|v|^2\right)^T, \ \langle g \rangle = \int_{\mathbb{R}^N} g(v)\, d_N v. \tag{3}$$

The physical quantity $E(x,t)$ is the total energy density, that is related to the temperature $T(x,t)$ by the underlying relation:

$$E(x,t) = \frac{1}{2}\rho(x,t)u(x,t)^2 + \frac{N}{2}\rho(x,t)RT(x,t).$$

The BGK model (1) satisfies the main properties of the Boltzmann equation [2,3], such as conservation of mass, momentum and energy, as well as entropy dissipation. In detail, for ϕ given in (3)

$$\langle M[f]\phi(v) \rangle = \langle f\phi(v) \rangle, \qquad \int_{\mathbb{R}^N} Q_{BGK}[f] \log f \, d_N v \leq 0. \tag{4}$$

The equilibrium solutions are clearly Maxwellians, indeed the collision operator vanishes for $f = M[f]$. The BGK model is computationally less expensive than the Boltzmann equation, due mainly to the simpler form of the collision operator, but it still provides qualitatively correct solutions for the macroscopic moments near the fluid regime (namely, when $\varepsilon \to 0$). These two aspects, the lower computational complexity and the correct description of the hydrodynamic limit, explain the interest in the BGK model over the last years (see for instance [5–8] and the references therein). Several numerical schemes have been recently proposed to solve the BGK equation in an efficient way, with particular attention to schemes that are able to capture the limiting behaviour of the solution as $\varepsilon \to 0$ (asymptotic preserving schemes, AP) [8–10]. The authors in [1] have proposed and investigated high order accurate schemes for the initial value problem (1) for the

BGK equation based on the semi-Lagrangian formulation. Semi-Lagrangian methods for BGK models have recently received increasing interest [11,12], since they well describe either a rarefied or a fluid regime. The relaxation operator has been treated implicitly and the semi-Lagrangian treatment of the convective part allows to avoid the classical CFL stability restriction. Time integration has been dealt with DIRK (Diagonally Implicit Runge Kutta) and BDF methods, and high orders in space have been obtained by suitable WENO reconstruction [13].
The aim of this paper is to include the treatment of boundary conditions into the high order semi-Lagrangian numerical schemes for the BGK equation developed in [1]; in particular, in this work we will focus on BDF methods, which turn out to be accurate but computationally less expensive than DIRK methods.
In many applications in rarefied gasdynamics the gas moves in a region D bounded by one or several solid bodies, and thus boundary conditions have to be prescribed to characterize the behaviour of the gas near the wall [4,14]. The first attempt to propose boundary conditions for the Boltzmann equation goes back to Maxwell in a paper published in 1879 [15], where he discussed the way to describe the interaction between a gas and a wall. The first hypothesis he proposed corresponds to a simple gas-solid interaction where he assumed that the wall is smooth, perfectly elastic and without any minute deviations, so that the gas particles are specularly reflected. The condition reads as:

$$f_s = \mathcal{R}[f(t,x,v)] = f(t,x,v-2n(v\cdot n)), \quad x\in\partial D,\ v\cdot n(x)\geq 0, \tag{5}$$

where $n(x)$ is the unit inward normal to the surface at x. Maxwell noticed that assumption (5), known as *specular reflection* boundary condition, means that the gas can exert stress on the surface only in the direction of the normal. This assumption is extremely unrealistic and can be only used in particular cases, since in many situations the gas can exert stress also in oblique directions to the surface, that cannot be represented as perfectly reflected. This is why he introduced another type of boundary conditions, corresponding to a more complex gas-solid interaction. As a second model for a real wall, Maxwell considered a stratum in which fixed elastic spheres are placed so far apart from one another that any one sphere is not sensibly protected by any other from the impact of molecules. Moreover the stratum is assumed to be deep enough so that every molecule going from the gas to the wall must collide once or more with the spheres. In this case, the particle is reflected into the gas with a velocity taken with a probability whose density corresponds to the gas in thermodynamical equilibrium with

the wall. In this case the boundary condition reads as

$$f_d = \mathcal{M}[f(t,x,v)] = \frac{\rho_b}{2\pi RT_b} \exp\left(-\frac{v^2}{2RT_b}\right), \quad x \in \partial D,\ v \cdot n(x) \geq 0, \tag{6}$$

where T_b is the temperature of the wall, and the value of ρ_b is determined by mass conservation at the surface of the wall for any $t \in \mathbb{R}^+$ and $x \in \partial D$

$$\frac{\rho_b}{2\pi RT_b} \int_{v\cdot n(x)\geq 0} \exp\left(-\frac{v^2}{2RT_b}\right) v \cdot n(x)\, dv = \tag{7}$$

$$= -\int_{v\cdot n(x)<0} f(t,x,v) v \cdot n(x)\, dv.$$

This model is known as *diffusive reflection* boundary condition. Finally, Maxwell proposed a more realistic model of boundary conditions, intermediate between the two previous ones. He postulated that there is a fraction of the gas which accommodates to the temperature of the wall and another one which is reflected by the solid and obtained the mixed boundary condition, that reads:

$$f(t,x,v) = (1-\alpha)\mathcal{R}[f(x,v,t)] + \alpha\mathcal{M}[f(x,v,t)], \quad x \in \partial D,\ v\cdot n(x) \geq 0, \tag{8}$$

where $\alpha \in [0,1]$ is called the accommodation coefficient and represents the tendency of the gas to accommodate to the wall. It means that the fraction $(1-\alpha)$ of molecules satisfies specular boundary conditions whereas a fraction α satisfies diffusive boundary conditions. When $\alpha = 0$ we recover the specular boundary condition while when $\alpha = 1$ we recover the diffusive boundary condition.

The paper is organized as follows. In Section 2 the numerical methods used and developed in [1] are recalled; in Section 3 we investigate the treatment of reflective and diffusive boundaries; two ways of adapting semi-Lagrangian schemes to diffusive boundary conditions are illustrated, using or avoiding iterative procedures. In Section 4 we report the inverse Lax-Wendroff technique proposed in [16–18] and adopted by Filbet and Yang in the context of diffusive boundary conditions [19]; numerical results are presented and compared in Section 5 and conclusions and future developments are discussed in Section 6.

2. Lagrangian formulation and numerical schemes.

We shall consider the BGK equation in one space and velocity dimension (namely $d = N = 1$ in (1),(2)). In the Lagrangian formulation, the time

evolution of $f(x, v, t)$ along the characteristic lines is given by the following system:

$$\begin{aligned} &\frac{df}{dt} = \frac{1}{\varepsilon}(M[f] - f), \\ &\frac{dx}{dt} = v, \\ &x(0) = \tilde{x}, \quad f(x, v, 0) = f_0(x, v), \qquad t \geq 0, \quad x, v \in \mathbb{R}. \end{aligned} \tag{9}$$

For simplicity, we assume constant time step Δt and uniform grid in physical and velocity space, with mesh spacing Δx and Δv respectively, and denote the grid points by $t^n = n\Delta t$, $x_i = x_0 + i\Delta x$, $i = 0, \ldots, N_x$, $v_j = j\Delta v$, $j = -N_v, \ldots, N_v$, where $N_x + 1$ and $2N_v + 1$ are the number of grid nodes in space and velocity respectively, so that $[x_0, x_{N_x}]$ is the space domain. We also denote the approximate solution $f(x_i, v_j, t^n)$ by f_{ij}^n.
Relaxation time ε is typically of the order of the Knudsen number, defined as the ratio between the molecular mean free path length and a representative macroscopic length; thus, the Knudsen number can vary in a wide range, from order greater than one (in rarefied regimes) to very small values (in fluid dynamic regimes). For this reason, if we want to capture the fluid-dynamic limit, we have to use an L-stable scheme in time.

2.1. *First order scheme*

An implicit first order L-stable semi-Lagrangian scheme (Figure 1) can be achieved in this simple way

$$f_{ij}^{n+1} = \tilde{f}_{ij}^n + \frac{\Delta t}{\varepsilon}(M[f]_{ij}^{n+1} - f_{ij}^{n+1}). \tag{10}$$

The quantity $\tilde{f}_{ij}^n \simeq f(x_i - v_j\Delta t, v_j, t^n)$ can be computed by suitable reconstruction from $\{f_{\cdot j}^n\}$; linear reconstruction will be sufficient for first order scheme, while higher order reconstructions, such as ENO or WENO [13], must be used to achieve high order avoiding oscillations. The convergence of this first order scheme has been studied in [12]. $M[f]_{ij}^{n+1}$ is the discrete Maxwellian constructed with the macroscopic moments of f^{n+1}:

$$M[f]_{ij}^{n+1} = M[f](x_i, v_j, t^{n+1}) = \frac{\rho_i^{n+1}}{\sqrt{2\pi R T_i^{n+1}}} \exp\left(- \frac{(v_j - u_i^{n+1})^2}{2RT_i^{n+1}} \right).$$

This formula requires the computation of the discrete moments of f^{n+1}, through a numerical approximation of the integrals in (3). This is obtained

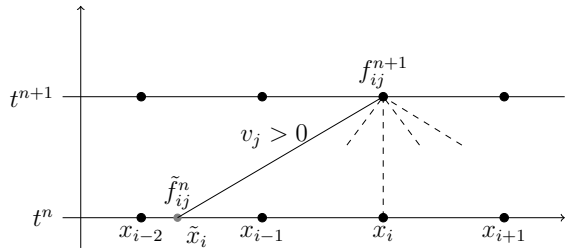

Figure 1. Representation of the implicit first order scheme. The foot of the characteristic does not lie on the grid, and some interpolation is needed to compute $\tilde{f}_{ij}^n$.

in the following standard way (see [1] for more details)

$$\rho_i^{n+1} = \sum_{j=-N_v}^{N_v} f_{ij}^{n+1}\Delta v, \qquad u_i^{n+1} = \frac{1}{\rho_i^{n+1}} \sum_{j=-N_v}^{N_v} v_j f_{ij}^{n+1}\Delta v, \tag{11}$$

$$E_i^{n+1} = \sum_{j=-N_v}^{N_v} \frac{1}{2} v_j^2 f_{ij}^{n+1}\Delta v.$$

From now on, we will denote formulas in (11) with the more compact notation: $(\rho_i^{n+1}, (\rho u)_i^{n+1}, E_i^{n+1}) = m[f_{i\cdot}^{n+1}]$, where, in general, $m[f]$ will indicate the approximated macroscopic moments related to the distribution function f.

It is evident that Equation (10) cannot be immediately solved for f_{ij}^{n+1}. It is a non linear implicit equation because the Maxwellian depends on f^{n+1} itself through its moments. To solve this implicit step one can act as follows. Let us take the moments of Equation (10); this is obtained at the discrete level by multiplying both sides by $\phi_j \Delta v$, where $\phi_j = \{1, v_j, v_j^2\}$ and summing over j as in (11). Then we have

$$\Delta v \sum_j (f_{ij}^{n+1} - \tilde{f}_{ij}^n)\phi_j = \Delta v \frac{\Delta t}{\varepsilon} \sum_j (M[f]_{ij}^{n+1} - f_{ij}^{n+1})\phi_j,$$

which implies that

$$\sum_j f_{ij}^{n+1}\phi_j = \sum_j \tilde{f}_{ij}^n \phi_j,$$

because, by definition, the Maxwellian at time t^{n+1} has the same moments as f^{n+1} and we assume that Equations (11) is accurate enough so that exact moments are well approximated by the discrete sum in (11). Indeed

Equations (11) provide spectral accuracy for smooth functions on compact support [6]. Thus we get

$$m[f_{i\cdot}^{n+1}] \simeq m[\tilde{f}_{i\cdot}^{n}]. \tag{12}$$

Once the Maxwellian at time t^{n+1} is known using the approximated macroscopic moments $m[\tilde{f}_{i\cdot}^{n}]$, the distribution function f_{ij}^{n+1} can be explicitly computed

$$f_{ij}^{n+1} = \frac{\varepsilon \tilde{f}_{ij}^{n} + \Delta t M_{ij}^{n+1}}{\varepsilon + \Delta t}. \tag{13}$$

This approach has been already used in [12,20], and in [8] in the context of Eulerian schemes.

2.2. *BDF method.*

The scheme of the previous section corresponds to implicit Euler applied to the BGK model in characteristic form. High order discretization in time can be obtained by DIRK or BDF methods [1].

Here the characteristic formulation of the BGK model, that leads to ordinary differential equations, is approximated by using BDF2, in order to obtain second order approximation. The relevant expression, under the hypothesis that the time step Δt is fixed, is (see Figure 2):

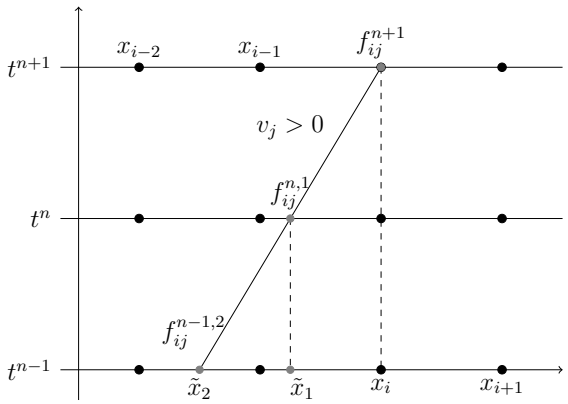

Figure 2. Representation of the BDF2 scheme. The black circles denote grid nodes, the gray ones the points where interpolation is needed.

$$\text{BDF2} := \quad f_{i,j}^{n+1} = \frac{4}{3} f_{ij}^{n,1} - \frac{1}{3} f_{ij}^{n-1,2} + \frac{2}{3} \frac{\Delta t}{\varepsilon} (M[f]_{ij}^{n+1} - f_{ij}^{n+1}), \tag{14}$$

where $f_{i,j}^{n-(s-1),s} \simeq f(t^{n-(s-1)}, x_i - sv_j\Delta t, v_j)$ can be computed by suitable reconstruction from $\{f_{\cdot j}^{n-(s-1)}\}$; we make use of WENO techniques [13] for accurate non oscillatory reconstruction.

Algorithm (BDF2)

- Calculate $f_{ij}^{n-1,2} = \tilde{f}(t^{n-1}, \tilde{x}_2 = x_i - 2v_j\Delta t, v_j)$, $f_{ij}^{n,1} = \tilde{f}(t^n, \tilde{x}_1 = x_i - v_j\Delta t, v_j)$ by interpolation from $f_{\cdot j}^{n-1}$ and $f_{\cdot j}^{n}$ respectively;
- Compute the Maxwellian $M[f_{ij}^{n+1}]$ by means of $m[\frac{4}{3}f_{i\cdot}^{n,1} - \frac{1}{3}f_{i\cdot}^{n-1,2}]$ and upgrade the numerical solution f_{ij}^{n+1} using (14).

3. Numerical treatment of the boundary conditions.

3.1. *Specular reflection.*

For the sake of simplicity we suppose that the wall is placed in $x_b = 0$. Each particle hitting the wall is immediately reflected by the wall with the same tangential velocity and opposite normal velocity:

$$v_{\text{refl}} = v - 2n(v \cdot n)$$

where v_{refl} is the particle velocity after reflection and v the particle velocity before reflection. This holds true for each particle such that $v \cdot n(x_b) \geq 0$. For $v \cdot n(x_b) < 0$, the distribution function on the boundary is already known from the inner cell. The distribution function for the boundary points has to be computed only for $v \cdot n(x_b) > 0$. Therefore the numerical discretiza-

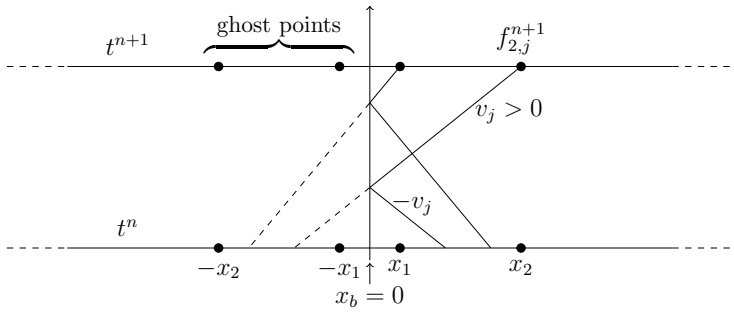

Figure 3. Discretization of specular reflective conditions.

tion of the specular reflective condition is very easy. In order to extend the distribution function beyond the wall, for the first order scheme (10) it is sufficient to use a number of ghost points equal to the smallest integer greater or equal to the CFL number. The ghost points will be placed symmetrically with respect to the wall, and, if $x_g = -x_k$ is the ghost point

symmetric to x_k, the value of the distribution function on x_g will be $f^n_{k,-j}$, whereas in x_k one has $f^n_{k,j}$. In this way we can compute the feet of the characteristics by considering the extension of the impinging characteristics (dashed lines in Figure 3) beyond the wall without using the reflected characteristics.
The extension to high order accuracy can be achieved in analogous way; in details, if we use BDF2, the characteristics have to be traced until time t^{n-1}; then, the number of ghost points will be double respect to the first order scheme. To interpolate in space we use the WENO approach of second order accuracy developed in [13] and used in [1].

3.2. *Diffusive reflection.*

Now we focus on the numerical approximation of solutions of kinetic BGK equations in presence of diffusive reflection boundary conditions. We propose two techniques: the first is based on an iterative procedure, the second one avoids the iterative procedure. The proposed techniques do not make use of ghost points. For simplicity, in Figure 4 the wall is located on a grid node, but the scheme can be easily adapted also to the case in which the wall is not on a grid node.

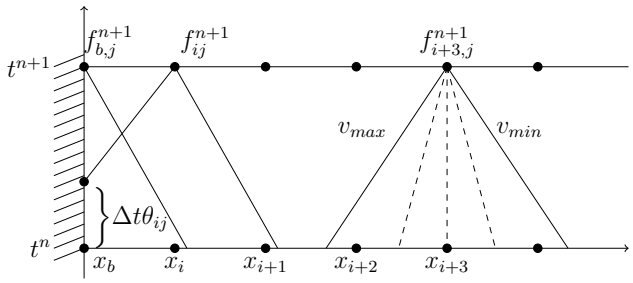

Figure 4. Discretization of diffusive conditions. We can distinguish inner nodes (for instance x_{i+3}), whose characteristics fan do not touch the wall, nodes located on the wall (x_b), and nodes for which only a part of the characteristics fan touches the wall (e.g. x_i).

3.2.1. *Approach using an iterative procedure (IP).*

We have to consider three types of spatial nodes: those that are far enough from the wall, for which the characteristics fan does not touch the wall (inner nodes); nodes sufficiently close to the wall, for which only a part of the characteristics fan touches the wall, and then nodes located at the wall, for which a special treatment is needed.
In the inner nodes f^{n+1} can be computed using the standard procedure described in Section 2. Now we compute the values of the distribution function

on the wall. Let us assume that the boundary is located on the left, at position $x_b = 0$ with temperature T_b. Let us consider the first order scheme; we assume that the solution at time t^n: $\left\{ f_{ij}^n, i = 0, \dots, N_x,\ j = -N_v, \dots, N_v \right\}$ is known, together with the density at $x_b = 0$, ρ_b^n. The density ρ_b^{n+1} is computed by imposing zero mass flux at $t = t^{n+1}$, $x_b = 0$, that is

$$\rho_b^{n+1} = \frac{-\sum_{v_j \cdot n(x_b) < 0} v_j \cdot n(x_b) f_{bj}^{n+1}}{\sum_{v_j \cdot n(x_b) \geq 0} v_j \cdot n(x_b) G_{bj}}, \tag{15}$$

where

$$f_{bj}^{n+1} = \begin{cases} \rho_b^{n+1} G_{bj} & \text{if } v_j \cdot n(x_b) \geq 0, \\ \\ \tilde{f}_{ij}^n + \dfrac{\Delta t}{\varepsilon}(M_{bj}^{n+1} - f_{bj}^{n+1}) & \text{if } v_j \cdot n(x_b) < 0, \end{cases} \tag{16}$$

with $G_{bj} = \exp(-v_j^2/2RT_b)/(2\pi RT_b)^{1/2}$. The quantity $\tilde{f}_{ij}^n \simeq f(x_i - v_j \Delta t, v_j, t^n)$ is a suitable reconstruction of $\{f_{\cdot j}^n\}$, as stated above. The half-space Maxwellian M_{bj}^{n+1} cannot be computed using (12), because it is defined only for $v_j \cdot n(x_b) \geq 0$. Thus, we are not able to compute the macroscopic moments of $(M_{b\cdot}^{n+1} - f_{b\cdot}^{n+1})$ by summing on the whole domain of velocities, as needed to obtain (12). In order to not alter the semi-lagrangian method developed in [1], a natural way to proceed is through an iterative procedure, which is simple to implement and physically sound. Let

$$f_{bj}^{(0)} = \begin{cases} \rho_b^{(0)} G_{bj} & \text{if } v_j \cdot n(x_b) \geq 0, \\ \\ \tilde{f}_{ij}^n = f(t^n, x_i - v_j \Delta t, v_j) & \text{if } v_j \cdot n(x_b) < 0. \end{cases}$$

Imposing $\sum_j v_j f_{bj}^{(0)} = 0$ one determines $\rho^{(0)}$. Once $\rho^{(0)}$ is known, one computes the moments $m^{(0)} = m[f_{b\cdot}^{(0)}]$. From the moments $m^{(0)}$ one computes the Maxwellian $M_{bj}^{(0)}$. Then one can iterate until convergence:

$$f_{bj}^{(k)} = \begin{cases} \rho_b^{(k)} G_{bj} & \text{if } v_j \cdot n(x_b) \geq 0, \\ \\ \tilde{f}_{ij}^n + \dfrac{\Delta t}{\varepsilon}(M_{bj}^{(k-1)} - f_{bj}^{(k)}) & \text{if } v_j \cdot n(x_b) < 0. \end{cases}$$

Finally we set $f_{bj}^{n+1} = \lim_{k \to \infty} f_{bj}^{(k)}$ and $\rho_b^{n+1} = \lim_{k \to \infty} \rho_b^{(k)}$. Once the density at time t^{n+1} has been found on the wall, one can then compute the

function at other grid points as follows. Let us consider, for example, point x_i in the previous Figure 4. Then one has:

$$f_{ij}^{n+1} = \begin{cases} \tilde{f}_{ij}^{n} + \dfrac{\Delta t}{\varepsilon}(M_{ij}^{n+1} - f_{ij}^{n+1}) & \text{if } \tilde{x}_{ij} = x_i - v_j \Delta t \geq 0, \\ \\ f_{\theta_{ij}} = \big(\theta_{ij}\rho_b^{n+1} + (1-\theta_{ij})\rho_b^{n}\big) G_{bj} & \text{if } \tilde{x}_{ij} < 0. \end{cases} \tag{17}$$

$f_{\theta_{ij}}$ represents the value of f on the wall and along the characteristic starting from x_i with velocity v_j. The geometrical factor $\theta_{ij} = 1 - x_i/(v_j \Delta t)$ can be computed for each velocity.
The Maxwellian M_{ij}^{n+1} may be computed by using an iterative procedure similar to the one used for the computation of ρ_b^{n+1}. Starting from

$$f_{ij}^{(0)} = \begin{cases} \tilde{f}_{ij}^{n} & \text{if } \tilde{x}_{ij} \geq 0, \\ \\ f_{\theta_{ij}} & \text{if } \tilde{x}_{ij} < 0, \end{cases}$$

one computes the moments $m^{(0)} = m[f_{i\cdot}^{(0)}]$ and then $M_{ij}^{(0)}$. Given $f_{ij}^{(k-1)}$, compute

$$f_{ij}^{(k)} = \begin{cases} \tilde{f}_{ij}^{n} + \dfrac{\Delta t}{\varepsilon}(M_{ij}^{(k-1)} - f_{ij}^{(k)}) & \text{if } \tilde{x}_{ij} \geq 0, \\ \\ f_{\theta_{ij}} & \text{if } \tilde{x}_{ij} < 0. \end{cases}$$

Finally we set $f_{ij}^{n+1} = \lim_{k\to\infty} f_{ij}^{(k)}$.

Here we show how to obtain a second order treatment of the boundary. The extension to high order is analogous and does not present particular difficulties. Using the BDF2 scheme presented in the previous section and in [1] we have

$$f_{bj}^{n+1} = \begin{cases} \rho_b^{n+1} \dfrac{\exp(-v_j^2/2RT_b)}{(2\pi RT_b)^{1/2}} & \text{if } v_j \cdot n(x_b) \geq 0, \\ \\ \dfrac{4}{3} f_{ij}^{n,1} - \dfrac{1}{3} f_{ij}^{n-1,2} + \dfrac{2\Delta t}{3\varepsilon}\big(M_{bj}^{n+1} - f_{bj}^{n+1}\big) & \text{if } v_j \cdot n(x_b) < 0. \end{cases} \tag{18}$$

The Maxwellian M_{bj}^{n+1} is obtained again by means of an iterative procedure.

Let

$$f_{bj}^{(0)} = \begin{cases} \rho_b^{(0)} G_{bj} & \text{if } v_j \cdot n(x_b) \geq 0, \\ \\ \dfrac{4}{3} f_{ij}^{n,1} - \dfrac{1}{3} f_{ij}^{n-1,2} & \text{if } v_j \cdot n(x_b) < 0. \end{cases}$$

with $G_{bj} = \exp(-v_j^2/2RT_b)/(2\pi RT_b)^{1/2}$. Imposing $\sum_j v_j f_{bj}^{(0)} = 0$ one determines $\rho^{(0)}$. Once $\rho^{(0)}$ is known, one computes the moments $m^{(0)} = m[f_{b\cdot}^{(0)}]$. From the moments $m^{(0)}$ one computes the Maxwellian $M_{bj}^{(0)}$. Then one can iterate until convergence:

$$f_{bj}^{(k)} = \begin{cases} \rho_b^{(k)} G_{bj} & \text{if } v_j \cdot n(x_b) \geq 0, \\ \\ \dfrac{4}{3} f_{ij}^{n,1} - \dfrac{1}{3} f_{ij}^{n-1,2} + \dfrac{2\Delta t}{3\varepsilon} \big(M_{bj}^{(k-1)} - f_{bj}^{(k)} \big) & \text{if } v_j \cdot n(x_b) < 0. \end{cases}$$

Finally we set $f_{bj}^{n+1} = \lim_{k\to\infty} f_{bj}^{(k)}$ and $\rho_b^{n+1} = \lim_{k\to\infty} \rho_b^{(k)}$. Once the density at time t^{n+1} has been found on the wall, the function at other grid points is computed as follows:

(19)

$$f_{ij}^{n+1} = \begin{cases} \dfrac{4}{3} f_{ij}^{n,1} - \dfrac{1}{3} f_{ij}^{n-1,2} + \dfrac{2\Delta t}{3\varepsilon} \big(M_{ij}^{n+1} - f_{ij}^{n+1} \big) & \text{if } \tilde{x}_{ij} = x_i - 2v_j \Delta t \geq 0, \\ \\ f_{\theta_{ij}} & \text{if } \tilde{x}_{ij} < 0 \end{cases}$$

where $f_{\theta_{ij}}$ is the value of the distribution function in the point of intersection between the characteristic which start from x_i with velocity v_j and the wall. It is obtained by interpolation from f_{bj}^{n+1}, f_{bj}^{n} and f_{bj}^{n-1}. The parameter $0 \leq \theta_{ij} \leq 1$ tells us that the characteristic touches the wall after a time step equal to $2\theta_{ij}\Delta t$.

The Maxwellian M_{ij}^{n+1} may be computed by using an iterative procedure similar to the one used for the computation of ρ_b^{n+1}. Starting from

$$f_{ij}^{(0)} = \begin{cases} \dfrac{4}{3} f_{ij}^{n,1} - \dfrac{1}{3} f_{ij}^{n-1,2} & \text{if } \tilde{x}_{ij} \geq 0, \\ \\ f_{\theta_{ij}} & \text{if } \tilde{x}_{ij} < 0, \end{cases}$$

one computes the moments $m^{(0)} = m[f_{i\cdot}^{(0)}]$ and then $M_{ij}^{(0)}$. Given $f_{ij}^{(k-1)}$, compute

$$f_{ij}^{(k)} = \begin{cases} \dfrac{4}{3} f_{ij}^{n,1} - \dfrac{1}{3} f_{ij}^{n-1,2} + \dfrac{2\Delta t}{3\varepsilon}\left(M_{ij}^{(k-1)} - f_{ij}^{(k)}\right) & \text{if } \tilde{x}_{ij} \geq 0, \\ \\ f_{\theta_{ij}} & \text{if } \tilde{x}_{ij} < 0. \end{cases}$$

Finally we set $f_{ij}^{n+1} = \lim_{k\to\infty} f_{ij}^{(k)}$.

The main drawback of this approach is that it requires an iterative loops. Indeed, the iteration may be slow if $\varepsilon \ll \Delta t$ because, for instance for the first order scheme, one has:

$$f_{ij}^{(k)} = \begin{cases} \dfrac{\varepsilon \tilde{f}_{ij}^{n} + \Delta t M_{ij}^{(k-1)}}{\varepsilon + \Delta t} & \text{if } \tilde{x}_{ij} \geq 0, \\ \\ f_{\theta_{ij}} & \text{if } \tilde{x}_{ij} < 0, \end{cases}$$

and the coefficient $\dfrac{\Delta t}{\varepsilon + \Delta t}$ may be very close to 1.

An improvement can be achieved by the following technique that avoids iterative procedures.

3.2.2. *Approach without iterative procedure (EP).*

Let us assume that the boundary is located on the left, at position $x_b = 0$ with temperature T_b. We assume that the solution at time t^n, f^n, and the density at x_b, ρ_b^n, are known.
First of all, the distribution function at time t^{n+1} at points, that we will call *inner nodes*, for which the characteristics fan does not touch the wall (light gray region, Figure 5) can be computed using the technique described in Section 2. Then one can obtain the distribution function at the outflow region (dark gray region, Figure 5), where $v \cdot n(x_b) < 0$, for the spatial grid nodes whose characteristics fan touches the wall, by extrapolation. A natural way to extrapolate the distribution function is by using Lagrange polynomials. However, when a shock goes out of the boundary, the high order extrapolation may lead to severe oscillations near the shock. In such case, a lower order accurate but more robust extrapolation is needed to prevent oscillations. Therefore, a WENO type extrapolation [16,19] has been applied and will be described in the Appendix; however, a first order approach could be coupled with a linear extrapolation. We will denote by $f_{i,j}^{E,n+1}$ the distribution function obtained by extrapolation at time t^{n+1} in (x_i, v_j).

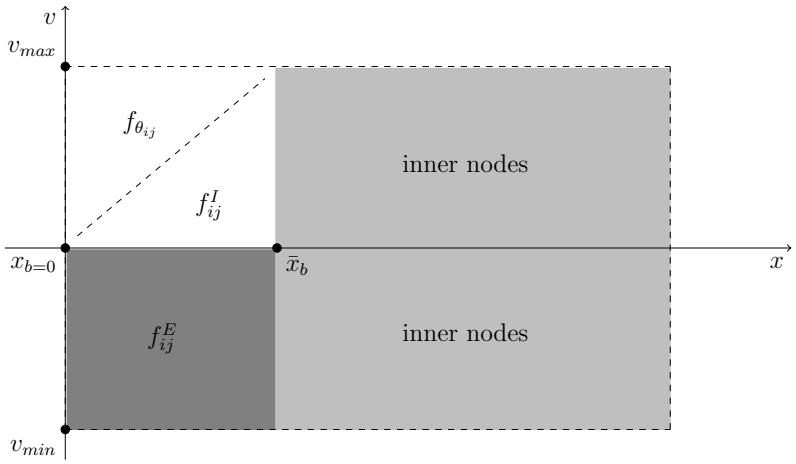

Figure 5. Mono dimensional phase space. The discretized distribution function is defined in $[x_b, +\infty] \times [v_{min}, v_{max}]$. The distances $|x_b - \bar{x}_b|$ is $v_{max}\Delta t$. Updating of the distribution function according with Equation (21). In the inner region (light gray) the characteristics fans do not touch the boundary. In the dark gray regions (outflow region, $v_j \cdot n(x_b) < 0$) we can extrapolate the distribution function from the inner region. For the inflow region (white region, $v_j \cdot n(x_b) \geq 0$) we use information coming from the wall.

Let us consider the first order scheme; we can compute the distribution function at the inflow boundary $v \cdot n(x_b) > 0$ in a very simple way, through a slight modification of the expression (16). We define the distribution function at the boundary in this way:

$$f_{bj}^{n+1} = \begin{cases} f_{bj}^{E,n+1} & \text{if } v_j \cdot n(x_b) < 0 \\ \\ \rho_b^{n+1} G_{bj} & \text{if } v_j \cdot n(x_b) \geq 0. \end{cases} \tag{20}$$

In Equation (20), extrapolation is used to obtain the values of f, instead of considering values along the characteristics for $v_j \cdot n(x_b) < 0$. In this way, the main difference between expressions (16) and (20) is that in (20) the Maxwellian at time t^{n+1} does not appear at all, therefore there is no need for iterative loops. The unknown is only ρ_b^{n+1}, that can be easily computed by (15) imposing zero mass flux at the boundary. At last, we have to update the distribution function at time t^{n+1} in the spatial grid nodes whose characteristics fan touches the wall at the inflow (white region,

Figure 5). In this case we define the distribution function as follows:

$$f_{ij}^{n+1} = \begin{cases} f_{ij}^{E,n+1} & \text{if } v_j \cdot n(x_b) < 0, \\ f_{\theta_{ij}} & \text{if } v_j \cdot n(x_b) \geq 0 \text{ and } \tilde{x}_{ij} < 0, \\ f_{ij}^{I,n+1} & \text{if } v_j \cdot n(x_b) \geq 0 \text{ and } \tilde{x}_{ij} > 0, \end{cases} \tag{21}$$

where $f_{ij}^{I,n+1}$ is obtained by a linear interpolation between f_{bj}^{n+1}, $f_{\theta_{ij}}$ on the left, and the value of f_{ij}^{n+1} in the inner nodes (light gray region in Figure 5) on the right.
Also in this case the main difference with respect to expression (17) is that in expression (21) the Maxwellian at time t^{n+1} does not appear, therefore there is no need for iterative loops to compute the macroscopic moments of the Maxwellian.
The main advantage of the EP technique respect to IP approach is that the computational time does not increase as the relaxation parameter tends to zero, but remains constant. The formulation is self consistent, mass conservation is maintained, and the numerical technique illustrated in Figure 5 has to be used only for few grid points near the boundary. Moreover, the extension to high order is very easy. It is enough to update f_{ij}^{n+1} at the inner nodes by high order schemes, like BDF2 for instance; then, to compute the outflow and inflow we proceed in the same way as described for the first order scheme, using now high order extrapolation (see Appendix) and high order interpolation [1,13].

The extrapolation techniques assume that the distribution function is smooth. For moderate values of ε this is a reasonable assumption, since usually discontinuities are introduced in the distribution function coming from the boundary, while we extrapolate from the inner region towards the boundary. As the Knudsen number becomes smaller and smaller, regions of large gradients may form (shocks), and the extrapolation procedure may be inaccurate if the grid does not resolve the shock or boundary layer. An additional advantage is that such a formulation is easily parallelizable: the extrapolated values can be computed in parallel, after updating the inner nodes and before the computation of the updated solution near the boundary.

4. Inverse Lax-Wendroff technique (ILW).

A technique already available in literature to treat diffusive boundary conditions, proposed by Shu and Tan [16] and adopted by Filbet and

Yang in the context of BGK model [19], is the Inverse Lax-Wendroff (ILW) method. This technique is useful when the numerical scheme requires ghost points, as in the case of IMEX schemes used in [19]. In particular, the ILW method is applied to compute the values of f at the ghost points for the inflow boundary. In this case we cannot approximate f by an extrapolation, since the distribution function at the interior points cannot predict the inflow. Filbet and Yang extended the ILW type procedure proposed in [16–18,21] for solving kinetic equations. At the boundary x_b, a first order Taylor expansion in space gives

$$f_j(x) = f_{x_b,j} + (x - x_b)\frac{\partial f}{\partial x}\bigg|_{x=x_b} + O(\Delta x^2).$$

Hence a first order approximation of f at ghost points x_g is

$$f_{g,j} = f_{x_b,j} + (x_g - x_b)\frac{\partial f}{\partial x}\bigg|_{x=x_b}.$$

To obtain the values at the ghost points it is necessary to approximate the first spatial derivative. By reformulating the BGK equation we have

$$\frac{\partial f}{\partial x}\bigg|_{x=x_b} = \frac{1}{v_x}\bigg(- \frac{\partial f}{\partial t} + \frac{1}{\varepsilon}(M[f] - f)\bigg)\bigg|_{x=x_b}.$$

Now, instead of approximating the first spatial derivative, one has to compute the time derivative and the collision operator in $x = x_b$. An approximation of the time derivative and of the collision term can be computed explicitly using the values of f at previous time instants at the boundary. In the numerical tests section a comparison between the technique proposed in this paper and the ILW method is performed. In our tests the ILW method is adopted in conjunction with the following second order IMEX scheme [7]

0	0	0	0
γ	γ	0	0
1	δ	1-δ	0
	δ	1-δ	0

0	0	0	0
γ	0	γ	0
1	0	1-γ	γ
	0	1-γ	γ

where $\gamma = 1 - \sqrt{2}/2$, $\delta = 1 - 1/(2\gamma)$.

5. Numerical tests.

In this section, we present a variety of test cases in 1D space-velocity showing the effectiveness of our methods to get an accurate solution of

Table 1. Relative errors and convergence rate of the distribution function in the whole domain, in L^2 norm using IP with CFL=0.45.

L_2 relative errors					
N_x	$\varepsilon = 1$	$\varepsilon = 10^{-1}$	$\varepsilon = 10^{-2}$	$\varepsilon = 5 \cdot 10^{-3}$	$\varepsilon = 10^{-3}$
80	1.644e-3	6.154e-4	2.815e-3	4.312e-3	8.990e-3
160	7.578e-4	1.921e-4	1.198e-3	1.826e-3	4.638e-3
320	2.206e-4	5.286e-5	4.544e-4	6.891e-4	1.584e-3
640	5.576e-5	1.392e-5	1.667e-4	3.550e-4	8.387e-4
1280	1.381e-5	3.646e-6	6.524e-5	1.591e-4	5.219e-4
L_2 orders					
160	1.1176	1.6796	1.2322	1.2399	0.9547
320	1.7799	1.8616	1.3988	1.4059	1.5496
640	1.9845	1.9250	1.4469	0.9568	0.9178
1280	2.0127	1.9327	1.3535	1.1579	0.6843

Table 2. Relative errors and convergence rate of the distribution function at the boundary, in L^2 norm using IP with CFL=0.45.

L_2 relative errors at the boundary					
N_x	$\varepsilon = 1$	$\varepsilon = 10^{-1}$	$\varepsilon = 10^{-2}$	$\varepsilon = 5 \cdot 10^{-3}$	$\varepsilon = 10^{-3}$
160	7.076e-5	2.792e-4	2.707e-3	3.702e-3	5.253e-3
320	1.795e-5	7.551e-5	1.028e-3	1.411e-3	2.377e-3
640	4.513e-6	1.761e-5	3.312e-4	4.594e-4	4.029e-4
1280	1.120e-6	4.181e-6	9.314e-5	1.445e-4	1.207e-4
L_2 orders at the boundary					
320	1.9787	1.8864	1.3959	1.3914	1.1440
640	1.9922	2.1003	1.6351	1.6192	2.5605
1280	2.0103	2.0745	1.8302	1.6684	1.7389

Table 3. Relative errors and convergence rate of the distribution function in the whole domain, in L^2 norm using IP with CFL=1.5.

L_2 relative errors					
N_x	$\varepsilon = 1$	$\varepsilon = 10^{-1}$	$\varepsilon = 10^{-2}$	$\varepsilon = 5 \cdot 10^{-3}$	$\varepsilon = 10^{-3}$
80	1.536e-3	4.032e-4	1.539e-3	3.121e-3	9.630e-3
160	6.486e-4	1.173e-4	8.530e-4	1.728e-3	6.334e-3
320	1.647e-4	3.643e-5	5.314e-4	1.019e-3	2.915e-3
640	3.852e-5	1.573e-5	3.019e-4	5.645e-4	1.623e-3
1280	9.763e-6	7.852e-6	1.633e-4	3.007e-4	8.621e-4
L_2 orders					
160	1.2445	1.7803	0.8515	0.8525	0.6043
320	1.9775	1.6879	0.6826	0.7619	1.1195
640	2.0960	1.2112	0.8159	0.8525	0.8449
1280	1.9803	1.0030	0.8866	0.9084	0.9129

the BGK equation in a bounded domain with purely diffusive boundary conditions ($\alpha = 1$ in (8)). The results related to reflective conditions have been presented in [1]. The numerical results have been obtained using BDF2

Table 4. Relative errors and convergence rate of the distribution function at the boundary, in L^2 norm using IP with CFL=1.5.

L_2 relative errors at the boundary					
N_x	$\varepsilon = 1$	$\varepsilon = 10^{-1}$	$\varepsilon = 10^{-2}$	$\varepsilon = 5 \cdot 10^{-3}$	$\varepsilon = 10^{-3}$
160	5.962e-5	6.854e-5	1.900e-4	2.252e-4	1.761e-3
320	2.121e-5	2.028e-5	1.301e-4	7.660e-5	1.557e-3
640	8.531e-6	2.022e-5	1.033e-4	3.182e-5	6.692e-4
1280	3.744e-6	1.227e-5	6.911e-5	1.545e-5	2.433e-4
L_2 orders at the boundary					
320	1.4908	1.7567	0.5462	1.5558	0.1779
640	1.3142	0.0042	0.3330	1.2674	1.2182
1280	1.1882	0.7209	0.5800	1.0421	1.4598

scheme.

5.1. *Smooth solutions.*

First of all, we consider a smooth initial data to compute the order of convergence in L^2 norm of our numerical method. We consider a bounded spatial domain $[x_L, x_R]$ and a smooth initial datum

$$f_0(x,v) = \frac{\rho_0(x)}{2\pi} \exp\left(-\frac{v^2}{2}\right), \; x \in (-0.5, 0.5), \; v \in [-10, 10],$$

with a density $\rho_0(x) = 1 + 0.1\cos(2\pi x)$. We consider purely diffusive boundary conditions with a wall temperature $T_L = T_R = 1$. We perform several numerical simulations on a time interval $[0, t_f]$ with $t_f = 1$, $N_v = 20$, and an increasing number of nodes in space: $N_x = 40, 80, \ldots, 1280$. In Tables 1, 2, 3, 4 we compute the error and the accuracy order in L^2 norm (in the whole domain and at the boundary) of the numerical method with IP (see Sect. 3.2), when the Knudsen number ε varies from rarefied to hydrodynamic regimes, for two different values of CFL (CFL= 0.45 in Tables 1, 2, CFL= 1.5 in Tables 3, 4). Analogously, in Tables 5, 6, 7, 8 we compute the error and the accuracy order in L^2 norm of the EP method, for different Knudsen and larger CFL numbers, which can be considered for the EP method without loss of accuracy, contrary to IP. A comparison between the two techniques for the same CFL number (CFL=1) will be shown in the next test. The error is computed taking the differences between two solutions obtained by two different meshes, N_x and $2N_x$. We can clearly see the expected second order convergence in rarefied regime; as the Knudsen number becomes smaller, the order decreases. A degradation of the order of accuracy for small values of ε is common to several implicit methods for stiff problems. For a method or order p, standard truncation analysis only

states that the error is of $O(\Delta t/\varepsilon)$, which is not useful in the regimes in which $\varepsilon < \Delta t$. A more detailed analysis, based on the expansion in ε of the exact solution and of the numerical solution, allows to study the accuracy for small values of ε. Such analysis can be found, for example, in the classical book of Hairer and Wanner [22] for systems of ODE's. A similar analysis has been applied to IMEX Runge-Kutta schemes for hyperbolic systems with relaxation [23], thus providing not only the explanation of the phenomenon, but also a guideline to the construction of schemes with better uniform accuracy with respect to ε. In all such analyses one assumes that there is no initial or boundary layer, which would cause degradation of accuracy in any cases. Initial layers can be cured by adopting small time steps during the transient, while boundary layers require an adaptive grid, which is finer near the boundary. Even without initial or boundary layers, the analysis in [23] cannot be applied here as it is, because of the different structure of the numerical scheme, which is semi-Lagrangian and BDF. It would be interesting to perform similar analysis, with the hope that it leads to suggestion on how to improve the accuracy of the methods for small and intermediate values of ε, however such analysis is beyond the scope of the present paper.

Table 5. Relative errors and convergence rate of the distribution function in the whole domain, in L^2 norm, using EP, CFL=2.

L_2 relative errors						
N_x	$\varepsilon = 1$	$\varepsilon = 10^{-1}$	$\varepsilon = 10^{-2}$	$\varepsilon = 10^{-3}$	$\varepsilon = 5 \cdot 10^{-4}$	$\varepsilon = 10^{-4}$
80	1.830e-3	3.994e-4	2.550e-3	9.373e-3	1.075e-2	1.212e-2
160	8.675e-4	1.407e-4	9.453e-4	5.205e-3	6.969e-3	9.351e-3
320	2.612e-4	4.149e-5	3.004e-4	1.857e-3	3.054e-3	6.140e-3
640	6.823e-5	1.129e-5	1.003e-4	4.991e-4	8.882e-4	2.913e-3
1280	1.719e-5	2.974e-6	3.912e-5	2.384e-4	3.492e-4	9.321e-4
L_2 orders						
160	1.0770	1.5054	1.4317	0.8487	0.6257	0.3744
320	1.7314	1.7617	1.6538	1.4865	1.1901	0.6068
640	1.9369	1.8767	1.5826	1.8958	1.7818	1.0755
1280	1.9886	1.9257	1.3583	1.0660	1.3468	1.6442

5.2. *Flow generated by a temperature gradient.*

Now we consider a test case of more interesting physical meaning. We suppose to have a hot wall, that will generate a flow towards the interior. We consider a bounded spatial domain $[x_L, x_R]$ and the initial data is the one used in [19], that is

$$f_0(x,v) = \frac{\rho_0(x)}{2\pi} \exp\left(-\frac{v^2}{2}\right),\ x \in (-0.5, 0.5),\ v \in [-10, 10],$$

Table 6. Relative errors and convergence rate of the distribution function at the boundary, in L^2 norm, using EP, CFL=2.

L_2 relative errors at the boundary						
N_x	$\varepsilon = 1$	$\varepsilon = 10^{-1}$	$\varepsilon = 10^{-2}$	$\varepsilon = 10^{-3}$	$\varepsilon = 5 \cdot 10^{-4}$	$\varepsilon = 10^{-4}$
160	7.928e-5	1.953e-4	2.393e-3	9.746e-3	1.069e-2	1.065e-2
320	1.749e-5	5.152e-5	7.601e-4	4.690e-3	6.668e-3	8.459e-3
640	4.260e-6	1.104e-5	1.933e-4	7.558e-4	1.613e-3	4.351e-3
1280	1.016e-6	2.389e-6	4.344e-5	2.580e-4	4.067e-4	9.265e-4
L_2 orders at the boundary						
320	2.1803	1.9226	1.6547	1.0551	0.6816	0.3331
640	2.0377	2.2213	1.9753	2.6336	2.0473	0.9591
1280	2.0680	2.2095	2.1535	1.5507	1.9876	2.2316

Table 7. Relative errors and convergence rate of the distribution function in the whole domain, in L^2 norm, using EP, CFL=4.

L_2 relative errors						
N_x	$\varepsilon = 1$	$\varepsilon = 10^{-1}$	$\varepsilon = 10^{-2}$	$\varepsilon = 10^{-3}$	$\varepsilon = 5 \cdot 10^{-4}$	$\varepsilon = 10^{-4}$
80	2.803e-3	1.662e-3	6.590e-3	1.583e-2	1.708e-2	1.823e-2
160	1.601e-3	5.328e-4	2.885e-3	1.033e-2	1.222e-2	1.443e-2
320	7.076e-4	1.613e-4	1.026e-3	4.909e-3	6.664e-3	9.753e-3
640	2.398e-4	4.556e-5	3.540e-4	1.799e-3	2.782e-3	5.668e-3
1280	6.838e-5	1.213e-5	1.246e-4	5.713e-4	9.143e-4	2.494e-3
L_2 orders						
160	0.8074	1.6417	1.1917	0.6160	0.4828	0.3375
320	1.1784	1.7239	1.4905	1.0736	0.8758	0.5652
640	1.5611	1.8239	1.5360	1.4483	1.2602	0.7828
1280	1.8103	1.9083	1.5060	1.6549	1.6054	1.1841

Table 8. Relative errors and convergence rate of the distribution function at the boundary, in L^2 norm, using EP, CFL=4.

L_2 relative errors at the boundary						
N_x	$\varepsilon = 1$	$\varepsilon = 10^{-1}$	$\varepsilon = 10^{-2}$	$\varepsilon = 10^{-3}$	$\varepsilon = 5 \cdot 10^{-4}$	$\varepsilon = 10^{-4}$
160	3.012e-4	5.294e-4	5.047e-3	1.520e-2	1.742e-2	1.994e-2
320	7.176e-5	2.013e-4	2.197e-3	6.871e-3	8.201e-3	1.040e-2
640	1.754e-5	4.876e-5	7.093e-4	1.931e-3	2.344e-3	2.870e-3
1280	4.405e-6	9.080e-6	1.920e-4	5.068e-4	7.384e-4	9.022e-4
L_2 orders at the boundary						
320	2.0697	1.3944	1.1995	1.1462	1.0872	0.9391
640	2.0323	2.0461	1.6314	1.8309	1.8065	1.8579
1280	1.9938	2.4250	1.8852	1.9300	1.6667	1.6696

with a density $\rho_0(x) = 1$ and $T_0(x) = 1 + 0.44(x + 0.5)$, $x \in (-0.5, 0.5)$. We consider purely diffusive boundary conditions with wall temperatures $T_L = 1$ and $T_R = 1.44$. We perform numerical simulations on a time interval $[0, t_f]$ with t_f varying from one test to the other (varying the Knudsen

number the equilibrium is reached at different time), and we fix $N_v = 20$. In Figure 6 we compare the stationary density and temperature profiles for two different Knudsen numbers, by plotting the differences between the solutions obtained with IP, EP techniques (with $N_x = 50$) and a reference solution obtained by ILW method (with $N_x = 200$), using the same CFL =1 to ensure the applicability of all of them; the results show that the EP technique turns out to be more accurate than the IP one.

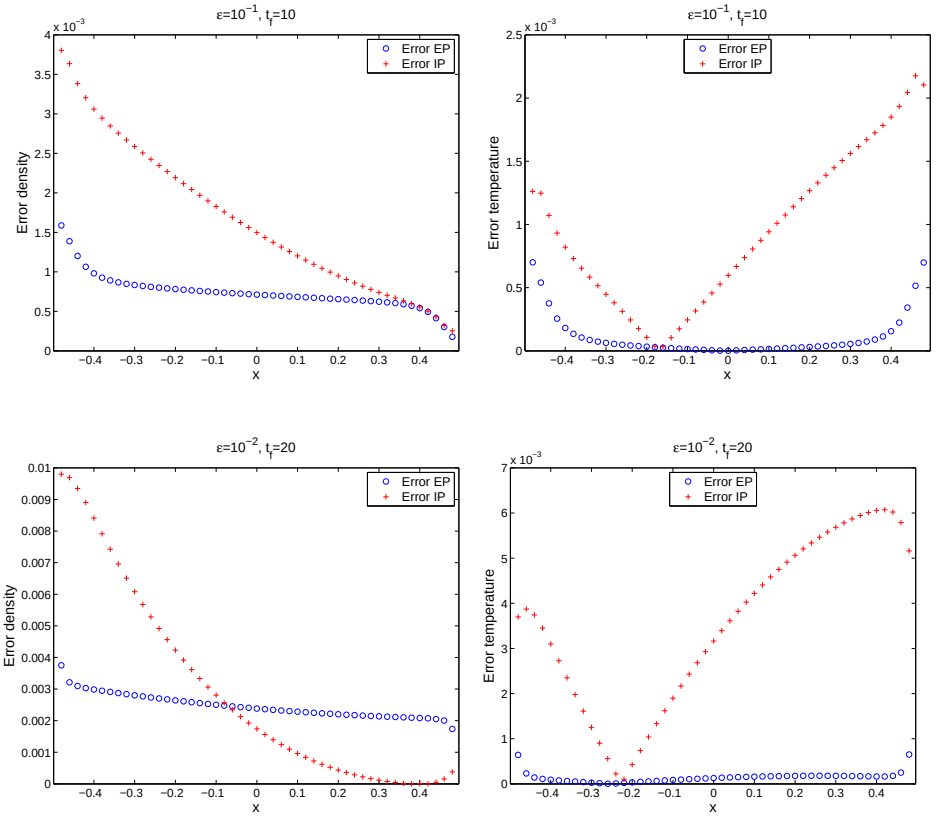

Figure 6. Error in density and temperature profiles generated by a temperature gradient obtained from IP and EP methods (with $N_x = 50$), at $t_f = 10$ if $\varepsilon = 10^{-1}$, and at $t_f = 20$ if $\varepsilon = 10^{-2}$,CFL=1, with respect to a reference solution obtained by ILW technique (with $N_x = 200$).

In Figure 7 we have the stationary profiles of density, temperature and pressure obtained with the EP approach. We perform numerical simulations on a time interval $[0, t_f]$ with t_f varying from one test to the other (varying the Knudsen number the equilibrium is reached at different time), $N_v = 20$, CFL number equal to 4 and $N_x = 100$. In Figure 7 we can see in particular the temperature and pressure profiles at different Knudsen numbers that are

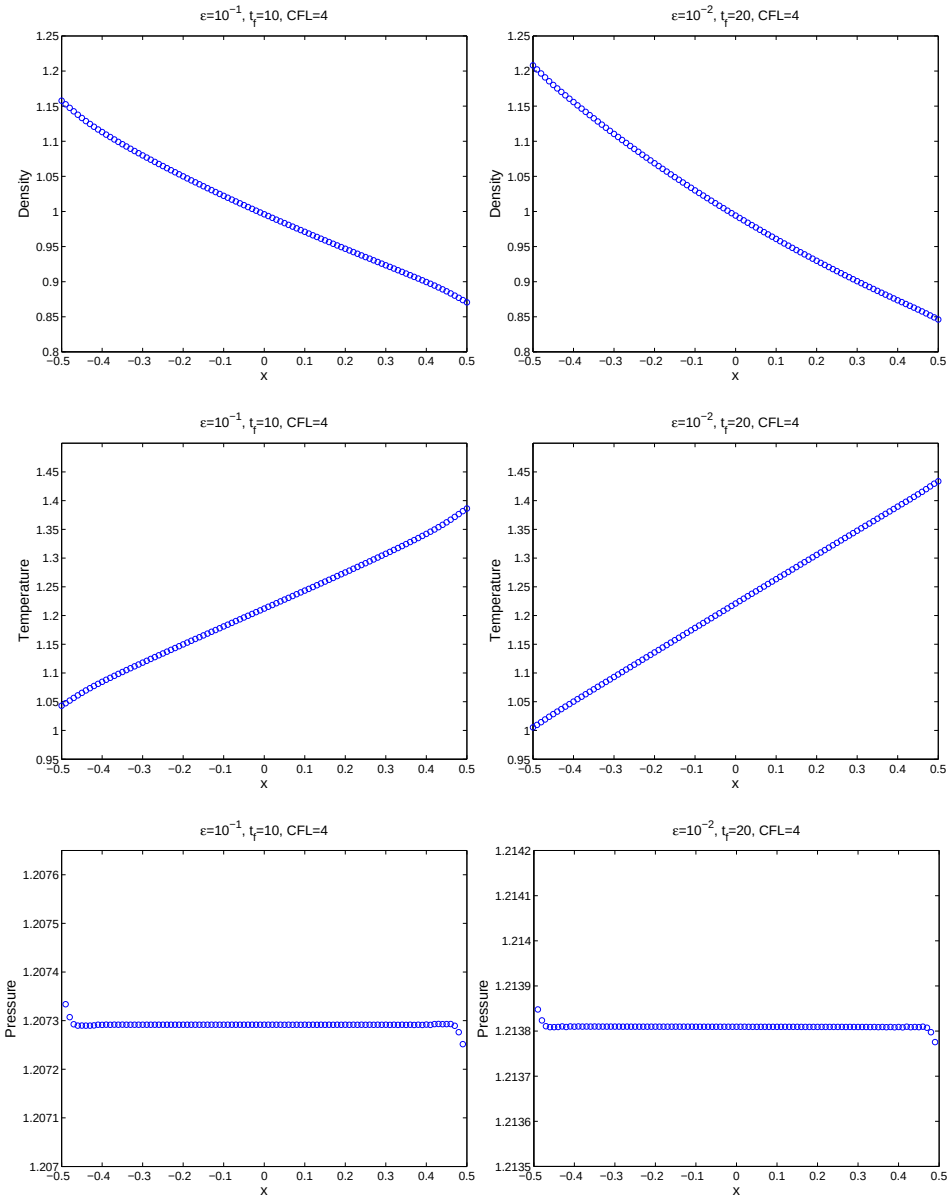

Figure 7. Stationary profiles of density, temperature and pressure, generated by a temperature gradient, obtained using EP technique at $t_f = 10$ if $\varepsilon = 10^{-1}$ (left) and at $t_f = 20$ if $\varepsilon = 10^{-2}$ (right), $N_x = 100$, CFL=4.

in good agreement with the results presented in [19] and obtained with the ILW method. A boundary layer (Knudsen layer) appears in the profiles of the macroscopic quantities; we can observe it without zoom in the pressure,

because its profile is almost constant in the bulk of the gas. Moreover, we can observe that the magnitude of the boundary layer is of order ε.

6. Conclusions and perspectives.

In this paper we have presented a second order approach for the numerical approximation of the space non homogeneous, time-dependent BGK equation in a bounded domain with different boundary conditions.
The method is an extension of the semi-Lagrangian schemes proposed in [1] to problems in bounded domains where reflective and diffusive boundary conditions are imposed.
Two approaches are proposed: one is based on an iterative procedure (IP) and the other is based on an extrapolation technique (EP). The IP procedure is physically more intuitive and may be easier to implement in some cases. However, the EP procedure works better than IP in terms of both accuracy and efficiency. Indeed, the EP technique gives more accurate results also for high CFL number (Tables 7, 8), that is using larger time step, and thus it preserves the main feature of schemes based on a semi-Lagrangian formulation.
Moreover, numerical tests show that the EP technique is reliable and efficient for small ε; the solution obtained by the ILW technique instead loses accuracy at the ghost points for small ε. The computational time needed for EP method does not increase as ε becomes smaller, contrary to what happens for IP technique, due to the growing number of iterations for ε approaching zero. These good properties of EP method suggest its application to other physical problems, like for instance the case of a binary mixture between two parallel planes reacting at the boundary [24].
The presented techniques can be generalized to two-dimensional (in space) problems, and some issues have to be considered. As regards specular reflection conditions, because of the discretization of the velocity space, one needs to compute $f(v_{\text{refl}})$, where in general v_{refl} does not correspond to a collocation point. In other words, even though v is a grid point, v_{refl} is not a velocity grid point except if the wall is parallel to the grid. Therefore $f(v_{\text{refl}})$ must be interpolated. The interpolation must be higher-order accurate to guarantee zero mass and energy fluxes at the wall with an acceptable degree of approximation. In the 1D case instead, it is enough to have a velocity grid symmetric with respect to $v = 0$ to avoid this problem. Moreover, in 2D, due to interpolation errors [25] mass and energy fluxes are not identically zero at the wall. This error leads to a boundary layer in the limit of inviscid gas simulations that should not exist. As shown in [25], to remove this spurious effect it is possible to use either a finer velocity grid

or a higher-order interpolation, at the price of significantly larger computational costs. As an alternative, the authors propose to use a Maxwellian reflected velocity that has zero net mass flux, temperature equal to molecule temperature, and mean velocity corresponding to specular reflection. Such conditions are compatible with inviscid conditions for Euler equations of gas dynamics, in the limit of zero Knudsen number. A similar approach for the treatment of specular reflection boundary conditions could be adopted with our semi-Lagrangian scheme.

As concerns diffusive boundary conditions, the EP technique is, with no doubt, easier to adapt to 2D problems with respect to the IP approach. Close to the wall, suitable extrapolation and interpolation 2D techniques allow to evaluate the solution without following the characteristics. The extension to high order is straightforward. At the inflow, where interpolation is used, it could be worthwhile to use ghost points outside the domain to improve the accuracy. The values of the distribution function in these points could be obtained using the ILW procedure developed by Filbet in [19] for the 2D case.

Appendix.

The WENO type extrapolation used for the treatment of diffusive boundary is the one developed in [16,17,19]. The key point of WENO type extrapolation is to define smoothness indicators, which are designed to balance the high order accuracy and the low order, but more robust, extrapolation.
Assume that we have a three points stencil $S = \{x_1, x_2, x_3\}$ and denote the corresponding distribution function by f_1, f_2, f_3. Instead of extrapolating f at the point x_{ex} by Lagrange polynomials, we use the following Taylor expansion

$$f_{ex} = \sum_{k=0}^{2} \frac{(x_{ex} - x_\ell)^k}{k!} \frac{d^k f}{dx^k}\bigg|_{x=x_\ell}.$$

We aim to obtain a $(3-k)$-th order approximation of $(d^k f/dx^k)\big|_{x=x_\ell}$ denoted by $f_\ell^{(k)}$, $k = 0, 1, 2$. Three candidate sub–stencils are given by

$$S_r = \{x_1, ..., x_{r+1}\},\ r = 0, 1, 2.$$

In each sub–stencil S_r, we could construct a Lagrange polynomial $p_r(x) \in \mathbb{P}_r(\mathbb{R})$

$$\begin{cases} p_0(x) = f_1, \\ p_1(x) = f_1 + \dfrac{f_2 - f_1}{\Delta x}(x - x_1), \\ p_2(x) = f_1 + \dfrac{f_2 - f_1}{\Delta x}(x - x_1) + \dfrac{f_3 - 2f_2 + f_1}{2\Delta x^2}(x - x_1)(x - x_2). \end{cases}$$

We now look for the WENO type extrapolation in the form

$$f_\ell^{(k)} = \sum_{r=0}^{2} \omega_r \frac{d^k p_r(x)}{dx^k}(x_\ell),$$

where ω_r are the nonlinear weights depending on f_i. We expect that $f_\ell^{(k)}$ is $(3-k)$–th order accurate in the case $f(x)$ is smooth. The nonlinear weights are given by

$$\omega_r = \frac{\alpha_r}{\sum_{s=0}^{2} \alpha_s},$$

with

$$\alpha_r = \frac{d_r}{(\delta + \beta_s)^2},$$

where $\delta = 10^{-6}$ and β_r are the new smoothness indicators determined by $\beta_0 = \Delta x^2$,

$$\beta_1 = (f_2 - f_1)^2,$$

$$\beta_2 = \frac{13}{12} f_1^2 + \frac{16}{3} f_2^2 + \frac{25}{12} f_3^2 - \frac{13}{3} f_1 f_2 + \frac{13}{6} f_1 f_3 - \frac{19}{3} f_2 f_3,$$

and $d_0 = \Delta x^2$, $d_1 = \Delta x$, and $d_2 = 1 - d_0 - d_1$. For more details see [16,17].

Acknowledgements. This work was supported by MIUR, by National Group of Computer Sciences (GNCS-INdAM), by National Group of Mathematical Physics (GNFM-INdAM), partially by the French-Italian program Galileo (project G14-34), and by the Universities of Catania and Parma (Italy).

REFERENCES

1. M. Groppi, G. Russo, and G. Stracquadanio, High order semilagrangian methods for bgk models, *Communications in Mathematical Sciences*, vol. 14, no. 2, pp. 389–414, 2015.

2. P. Bhatnagar, E. Gross, and K. Krook, A model for collision processes in gases, *Physical Review*, vol. 94, pp. 511–525, 1954.
3. P. Welander, On the temperature jump in a rarefied gas, *Arkiv för Fysik*, vol. 7, pp. 507–553, 1954.
4. C. Cercignani, *The Boltzmann Equation and its Applications*. Springer, 1988.
5. P. Andries, K. Aoki, and B. Perthame, A consistent bgk-type model for gas mixtures, *Journal of Statistical Physics*, vol. 106, pp. 993–1018, 2002.
6. L. Mieussens, Discrete velocity model and implicit scheme for the bgk equation of rarefied gas dynamics, *Mathematical Models and Methods in Applied Sciences*, vol. 10, pp. 1121–1149, 2000.
7. L. Pareschi and G. Russo in *Efficient asymptotic preserving deterministic methods for the Boltzmann equation*, AVT-194 RTO AVT/VKI, Models and Computational Methods for Rarefied Flows, Lecture Series held at the von Karman Institute, Rhode St. Genèse, Belgium, 24 -28 January 2011.
8. S. Pieraccini and G. Puppo, Implicit-explicit schemes for bgk kinetic equations, *Journal of Scientific Computing*, vol. 32, pp. 1–28, 2007.
9. G. Dimarco and R. Loubere, Towards an ultra efficient kinetic scheme. part ii: The high order case, *Journal of Computational Physics*, vol. 255, pp. 699–719, 2013.
10. S. Pieraccini and G. Puppo, Microscopically implicit-macroscopically explicit schemes for the bgk equation, *Journal of Computational Physics*, vol. 231, pp. 299–327, 2012.
11. F. Filbet and G. Russo, Semi-lagrangian schemes applied to moving boundary problems for the bgk model of rarefied gas dynamics, *Kinetic and Related Models*, vol. 2, pp. 231–250, 2009.
12. G. Russo, P. Santagati, and S.-B. Yun, Convergence of a semi-lagrangian scheme for the bgk model of the boltzmann equation, *SIAM Journal on Numerical Analysis*, vol. 50, pp. 1111–1135, 2012.
13. E. Carlini, R. Ferretti, and G. Russo, A weighted essentially nonoscillatory, large time-step scheme for hamilton-jacobi equations, *SIAM Journal on Scientific Computing*, vol. 27, pp. 1071–1091, 2005.
14. Y. Sone, *Kinetic Theory and Fluid Dynamics*. Birkäuser, 2002.
15. J. C. Maxwell, *The Scientific Parers of J. C. Maxwell*. Dover Publications, 1965.
16. S. Tan and C. Shu, Inverse lax-wendroff procedure for numerical boundary conditions of conservation laws, *Journal of Computational Physics*, vol. 229, pp. 8144–8166, 2010.

17. S. Tan, C. Wang, C. Shu, and J. Ning, Efficient implementation of high order inverse lax-wendroff boundary treatment for conservation laws, *Journal of Computational Physics*, vol. 231, pp. 2510–2527, 2012.
18. T. Xiong, M. Zhang, Y.-T. Zhang, and C.-W. Shu, Fast sweeping fifth order weno scheme for static hamilton-jacobi equations with accurate boundary treatment, *Journal of Scientific Computing*, vol. 45, pp. 514–536, 2010.
19. F. Filbet and C. Yang, An inverse lax-wendroff method for boundary conditions applied to boltzmann type models, *Journal of Computational Physics*, vol. 245, pp. 43–61, 2013.
20. P. Santagati, *High order semi-Lagrangian schemes for the BGK model of the Boltzmann equation*. PhD thesis, Department of Mathematics and Computer Science, University of Catania, 2007.
21. L. Huang, C.-W. Shu, and M. Zhang, Numerical boundary conditions for the fast sweeping high order weno methods for solving the eikonal equation, *Journal of Computational Mathematics*, vol. 26, no. 3, pp. 1–11, 2008.
22. E. Hairer and G. Wanner, *Solving Ordinary Differential Equations II: Stiff and Differential-Algebraic Problems*. Springer Series in Computational Mathematics 14, 1991.
23. S. Boscarino, Error analisysis of imex runge-kutta methods derived from differential-algebraic systems, *SIAM Journal on Numerical Analysis*, vol. 45, pp. 1600–1621, 2007.
24. M. Groppi, L. Desvillettes, and K. Aoki, Kinetic theory analysis of a binary mixture reacting on a surface, *The European Physical Journal B*, vol. 70, pp. 117–126, 2009.
25. F. Bernard, A. Iollo, and G. Puppo, Accurate asymptotic preserving boundary conditions for kinetic equations on cartesian grids, *Journal of Scientific Computing*, vol. 65, pp. 735–766, 2015.